Wideband and High Selectivity Dual-Band Filter for Ka-Band Satellite Antennas

Eduardo B. Lima, *IEEE Student Member*, Jorge R. Costa, *IEEE Senior Member*, Carlos A. Fernandes, *IEEE Senior Member*

***Abstract*— A dual-band miniaturized Ka-band filter is presented, taking advantage of transmission in cut-off rectangular waveguides periodically loaded in the E-plane with Split-Ring Resonators (SRRs). High selectivity, wide bandwidth and high out-of-band rejection are achieved in a compact form factor. The use of SRRs in a waveguide configuration proves to be a valid and promising solution for the design of dual-band filters. The filter is specifically designed for Ka-band and a prototype was manufactured and its performance measured, providing a reasonably flat transmission at both 20 and 30 GHz sub-bands. For both bands the power roll-off rate is higher than 55 dB/decade, translating into a sharper than 10 dB drop per 0.2 GHz in a 38 × 6.6 × 4.5 mm^3 device. The filter half-power bandwidth is B_{20} = 1.1 GHz at 20 GHz (18.4 - 19.5 GHz) and B_{30} = 1.2 GHz at 30 GHz (27.8 - 29.0 GHz).**

***Index Terms*— Split-ring resonator, dual-band filter, cut-off rectangular waveguide, E-plane loading, filter selectivity.**

I. Introduction

High Throughput Satellites (HTS) and particularly Ka-band satellite communication systems are presenting new challenges in space and ground segments [1]. Wideband and high selectivity dual-band filters are required in this context to cover both transmission and reception frequency bands. As an example for the space segment, its use is suggested in [2] to enable increasing the number of reflector feeds using polarization and frequency diversity. Since both 20 and 30 GHz frequency bands are divided into adjacent sub-bands, dual-wideband filters with high selectivity are mandatory to ensure proper isolation. To the authors' best knowledge, no dual-wideband and high selective filter is found in literature, which is dedicated for Ka-band satelitte systems.

A single-band filter with low selectivity is presented in [3], making use of a multilayer low-temperature co-fired ceramic (LTCC) structure. More recently, a Ka-band coupled-resonator filter, implementing gap waveguide technology was proposed to isolate the Tx and Rx channels [4]. Despite the sharp selectivity, it is single-band. Miniaturized and wideband bandpass filters with low insertion losses have been proposed in the literature, such as multi-mode resonators and split-ring resonators (SRRs) [5]-[6]. Nevertheless, these refer to single-band filters. Miniaturized dual-band filters, such as [7]-[8] could be scaled accordingly, but selectivity, bandwidth and frequency bands ratio are not compatible with Ka-band requirements. A varactor tunable dual-band bandpass filter using stub-loaded stepped-impedance resonators is proposed in [7], with close to 10 dB drop per 50 MHz at 900 MHz, which, at 20 GHz, would translate approximately to a 10 dB drop per 1 GHz, not providing proper isolation between adjacent sub-bands in Ka-band. A dual-band balun passband filter is shown in [8], but although high selectivity is achieved, it is a narrowband solution with 100 MHz bandwidth at 9 GHz with very close passbands, 9 and 9.8 GHz.

The transmission in SRR-loaded cut-off rectangular waveguides has been addressed in [9] to demonstrate "left-handed" media behavior. It shows a narrow pass-band with very high insertion losses. A different approach is presented in [10], where the coax-to-waveguide transition is designed directly in the cut-off section of the waveguide, near the SRR E-plane array. This allows extending the device test band far beyond the common waveguide bands. Simulations and measurements in [10] reveal a second pass-band with very small insertion loss, still below the waveguide cut-off frequency, which could be explored to produce compact filters. While the first resonance is associated with a "left-handed" behavior, the second resonance has a different nature, corresponding to a positive and high effective permittivity of the cut-off waveguide plus the SRRs assembly [10]. The present manuscript goes further proposing a dual-band filter with high selectivity, modifying the waveguide configuration.

II. Dual-Band Filter Design

The waveguide configuration is a modified version of [10], short-circuited at both ends and fed through a coaxial cable with the central conductor extended as a monopole probe, see Fig. 1. The waveguide contains an E-plane septum defining two sub-waveguides, for 20 GHz and 30 GHz each. SRRs are $\lambda/2$ resonant elements, with both inner and outer rings length being $\lambda/2$, with λ as the substrate loaded sub-waveguide wavelenght. The filter design followed the next guidelines:

Manuscript received July 2016. This work is supported by Research Networking Program NEWFOCUS of the European Science Foundation and it was supported in part by the Fundação para a Ciência e Tecnologia under Project mm-SatCom PTDC/EEI-TEL/0805/2012.

Eduardo B. Lima, Jorge R. Costa, and Carlos A. Fernandes are with Instituto de Telecomunicações, Instituto Superior Técnico, Universidade de Lisboa, Av. Rovisco Pais 1, 1049-001 Lisboa, Portugal (phone +351-218418480 fax +351-218418472 e-mail eduardo.lima@lx.it.pt).

Jorge R. Costa is also with Instituto Universitário de Lisboa (ISCTE-IUL), Departamento de Ciências e Tecnologias da Informação, Av. das Forças Armadas, 1649-026 Lisboa, Portugal.

a) SRRs loop length is $\approx \lambda/2$;
b) Distance between SRRs is $\approx \lambda/2$;
c) Distance between the waveguide short-circuit wall to probe is $\approx \lambda_0/4$ on both edges, with λ_0 as the wavelength in free space for the lower frequency band;
d) The number of SRR elements is given by the ratio between frequencies ($N_{f_1} = N_{f_2} * f_1/f_2$);
e) Waveguide height is defined by the largest SRR element;
f) Sub-waveguides' width corresponds to the minimum one that enables propagation at the pass-band.

The rectangular waveguide internal cross-section dimensions were optimized as 6.6 × 4.5 mm^2 ($a \times b$). The waveguide, with length L = 38 mm, is carved in Brass ($\sigma = 1.59\times10^7$ S/m). It is physically separated into two narrower parallel sub-waveguides by an E-plane metal wall of shorter length L_G = 26.8 mm, ending 2 mm off from the monopole probes located in the same plane, Fig. 1a). Considering the probe orientation, each sub-waveguide fundamental TE_{10} mode associated to the largest 4.5 mm dimension is not excited, being the cut-off frequency given by the TE_{01} mode. The 20 GHz sub-waveguide has an H-plane width a_{20} = 3.7 mm (cut-off frequency is $f_{c20} = 40.5\ GHz$) while the 30 GHz side has an H-plane width a_{30} = 2.9 mm ($f_{c30} = 51.7\ GHz$). The cut-off frequencies correspond to the lowest mode with no electric component along the x-axis.

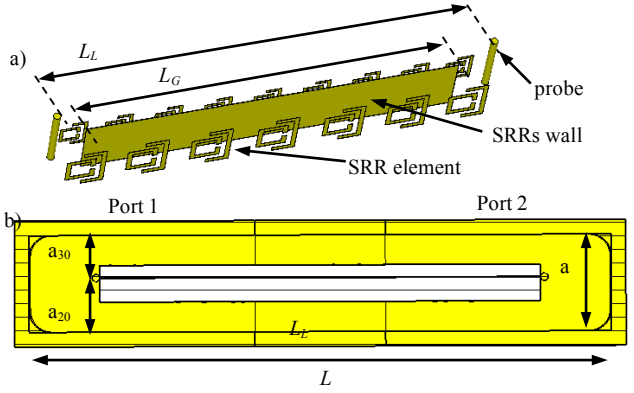

Fig. 1. Waveguide filter configuration: a) dual-band SRRs configuration; b) top view of the dual-band waveguide without top lid.

Each of these sub-waveguides is loaded in the E-plane with an array of SRRs printed on a substrate with copper ground plane on the other face ($\sigma = 5.8\times10^7$ S/m). The SRRs substrates, with a length L_L = 30.8 mm, are positioned with the respective ground planes coincident with the above referred central conducting wall. For clarity, the dielectric is made transparent in Fig. 1a). The substrate is Rogers 5880 (ε_r = 2.2, tan δ = 0.0009) with 1.575 mm thickness on the 20 GHz side and 0.787 mm thickness on the 30 GHz side. These SRR arrays produce a high effective permittivity loading that ensures propagation conditions in the 20 and 30 GHz sides.

The 20 GHz array of SRRs is centrally positioned with respect to the waveguide top and bottom walls, while the 30 GHz array of smaller SRRs' elements is shifted 0.6 mm upwards, enabling adequate coupling between the probe and the first SRR. The probes, with a diameter ∅ = 0.51 mm, length L_p = 2.7 mm are parallel to the SRRs plane and placed d_p = 3.85 mm off from the waveguide short-circuit wall, see Fig. 2. The position, diameter and length of the probes are of critical relevance, since they have to couple simultaneously with both arrays of SRRs, at very distinct bands.

The filter high selectivity is determined by the high number of SRRs on both sides, 7 elements for 20 GHz and 9 elements for 30 GHz. The choice of 7 elements instead of 6 allowed to increase the filter selectivity but the distance between elements becomes shorter than $\lambda/2$ as it will be shown ahead.

Circular ring is the common SRR configuration [9]-[11]; however, for design and analysis simplicity, a square geometry is adopted for both inner and outer square arms, see Fig. 2. In order to optimize the flatness and width of the pass band, the SRRs size and relative distance is not uniform. A scale factor is used to modify each SRR size with respect to the central one (the reference SRR, Table 1). The scale factors and distances between them are symmetrical with respect to the reference element (Table 2). The full length and distance between SRRs are shown in Table 3. *fli* and *flo* are the full length of the inner and outer rings of each SRR respectively.

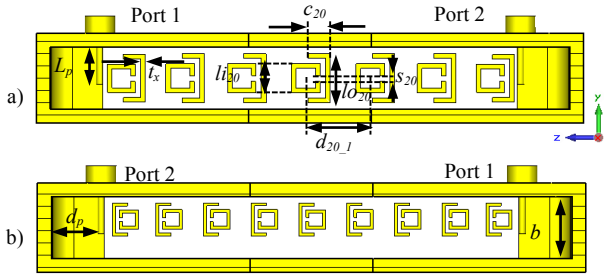

Fig. 2. Side-view of the waveguide filter: a) 20 GHz sub-waveguide; b) 30 GHz sub-waveguide.

Table 1. Dimensions of the reference element (see Fig. 2.a).

freq. [GHz]	Dimensions [mm]				
	lo_x	li_x	c_x	s_x	t_x
20	3.54	2.09	1.63	0.40	0.34
30	2.40	1.41	1.10	0.28	0.22

Table 2. Scale factor and distances between SRRs.

freq. [GHz]	Scale factor				Distance [mm]			
	sf_{x_1}	sf_{x_2}	sf_{x_3}	sf_{x_4}	d_{x_1}	d_{x_2}	d_{x_3}	d_{x_4}
20	1.002	1.002	0.973	-	4.69	4.49	4.30	-
30	1.005	1.005	1.007	1	3.49	3.49	3.49	3.17

Table 3. Full length and distance between SRRs.

freq. [GHz]	Full length [mm]		Distance [mm]
	fli_{x_1}	flo_{x_1}	d_{x_1}
20	$0.49 * \lambda_{19GHz}$	$0.51 * \lambda_{19GHz}$	$0.44 * \lambda_{19GHz}$
30	$0.51 * \lambda_{29GHz}$	$0.53 * \lambda_{29GHz}$	$0.50 * \lambda_{29GHz}$

The main design challenge is to achieve uncoupled propagation at the 20 and 30 GHz sub-waveguides with well-defined and separate band-pass regions. Besides these band-pass regions, each SRR-loaded sub-waveguide further exhibits a high-pass behavior that must be kept well beyond the band-pass region in both bands. The separation between these regions is critical for the 20 GHz subwaveguide where the high-pass cut-off frequency (f_{hp20}) must be higher than 30 GHz. Smaller a_{20} or c_{20} dimensions, thinner or lower

permittivity substrate shift up f_{hp20}. Another characteristic to consider is bandwidth, which, as with the high-pass cut-off frequency, is dependent of c_{20} and c_{30} values. Larger values of c_{20} and c_{30} shift the pass-band down but also decrease the bandwidth. The upper high-pass cut-off is more strongly affected by the c_x dimension than the lower cut-off frequency, allowing tuning the pass-band bandwidth.

To illustrate the abovementioned sub-waveguide independence, Fig. 3 presents the E-field magnitude on both sides of the waveguide for the central frequency of the two pass-bands, 19 and 29 GHz. The color scheme covers a 30 dB range. The E-field magnitude is represented at y = 1.75 mm, Fig. 3, coincident with both SRRs top arms. The 20 GHz sub-waveguide is not completely off at 29 GHz, Fig. 3b), but nearly 20 dB below the magnitude of the wave propagating on the 30 GHz side. On the other hand it is clear that at the 30 GHz side there is no propagation at 19 GHz, see Fig. 3a).

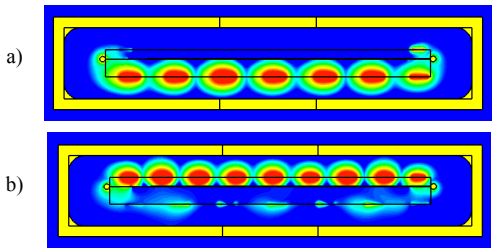

Fig. 3. Simulated E-field magnitude in the waveguide at y = 1.75 mm cut (approximate position of both SRRs top arm): a) 19 GHz; b) 29 GHz.

Fig. 4a) shows the corresponding s_{11} and s_{22}, slightly asymmetric due to the non-symmetric configuration of the SRR array. Two pass-bands are achieved, with central frequencies at 19 and 29 GHz and bandwidth larger than 1 GHz. The first and second pass-bands have 1.6 and 2.5 dB insertion loss respectively, Fig. 4b). Although some losses are due to the substrate, the main contribution comes from the SRRs material. Simulations show that the insertion loss reduces to ≈ 0.65 dB when the SRRs' copper is replaced by perfect electric conductive material (PEC) and drops to 0.3 dB when also considering lossless substrate.

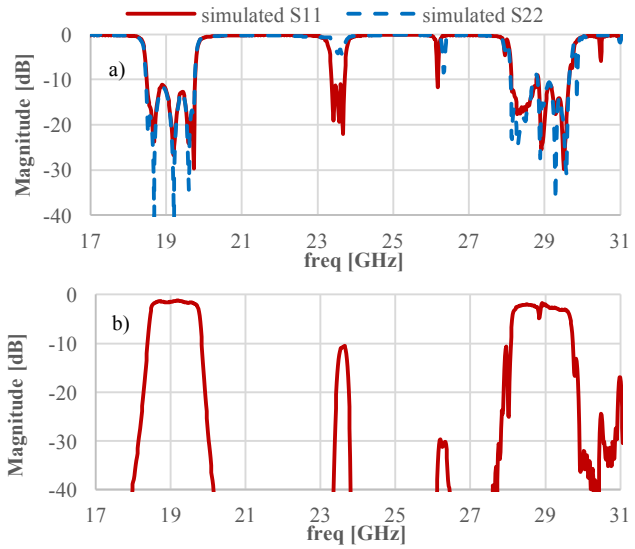

Fig. 4. Full-wave simulated filter response a) $|s_{11}|$, $|s_{22}|$ b) $|s_{21}|$.

There is an accentuated ripple at the 30 GHz band, not visible at the lower band, which is due to vestigial propagation at the 20 GHz sub-waveguide, interfering with the 30 GHz sub-waveguide propagation.

III. Prototype and Measurements

A prototype was manufactured with a waveguide consisting of three brass pieces, Fig. 5: a block with the carved waveguide, two closing lids and two coaxial probes. A mechanism was incorporated to allow fine control of the probe penetration in the waveguide. Measured and simulated s_{21} curves of the empty waveguide are shown in Fig. 6 as an intermediate control step. Good agreement is achieved, although the prototype already presents around 2 dB higher insertion losses than predicted. The discrepancy is probably due to imperfect cavity closing and probe inaccuracies.

Both SRR arrays were manufactured with printed circuit technology using Rogers 5880 substrate. The two arrays were glued with the respective ground planes facing each other, see Fig. 7a). In order to enforce conductivity between these ground planes and the waveguide top and bottom walls, the top and bottom faces of the SRRs block were painted with a conductive ink. SRRs' arrays are aligned inside the waveguide with a Styrofoam frame, Fig. 7b). This arrangement is prone to misalignment errors as well as conductivity issues; however, it was considered valid for the proof of concept.

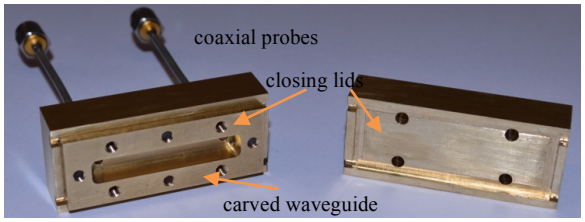

Fig. 5. Waveguide prototype of the dual-band filter.

Measurements showed a 1.5% frequency shift as well as transmission degradation. Further to the previously described limitations of the prototype, the anisotropy of the dielectric constant and loss tangent play a relevant role in this resonant structure. The previous filter was re-simulated considering the anisotropy values specified in the manufacturer data sheet [12]. Measurements are superimposed on the re-simulated waveguide results in Fig. 8 and Fig. 9. For simplicity, only s_{22} is presented but similar performance is obtained for s_{11}. The frequency agreement is significantly improved. Nevertheless, increased insertion loss is verified, 4 and 7 dB at 20 and 30 GHz bands, respectively. Two main factors contribute for the increased insertion losses: substrate anisotropy (3 dB at 30 GHz) and manufacturing innacuracies (empty cavity exhibits 2 dB of dissipated energy at 30 GHz, Fig. 6). A transmission drop in the middle of the 30 GHz band results from the proximity of the SRRs to the sub-waveguide top wall, becoming more evident when including the conductive ink, reducing the waveguide height. Two possibilities would allow eliminating the transmission drop, either shifting the SRRs elements down or by increasing the waveguide height in order to compensate the conductive ink thickness.

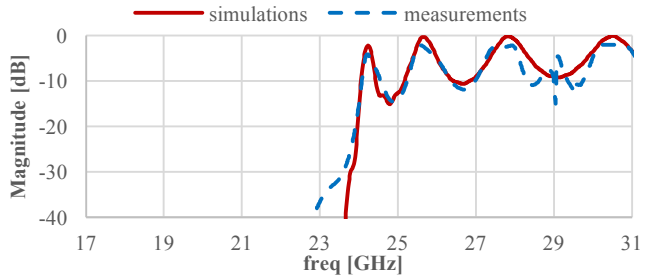

Fig. 6. S21 obtained with the cavity empty.

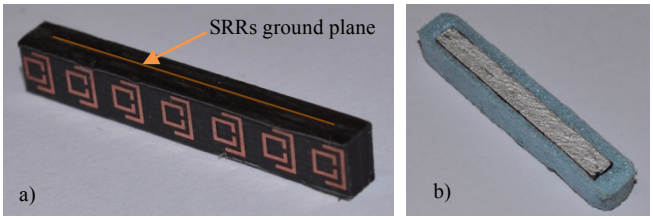

Fig. 7. Dual SRRs layer: a) prototype; b) with support and alignment Styrofoam, and top conductive ink.

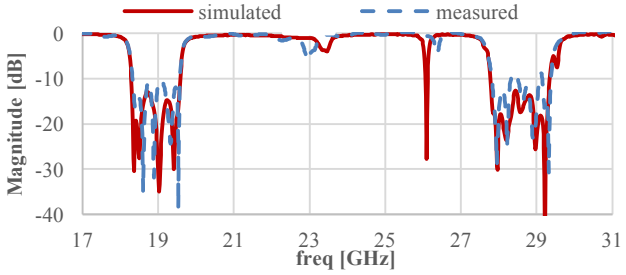

Fig. 8. Simulated and measured reflection coefficient, $|s_{22}|$.

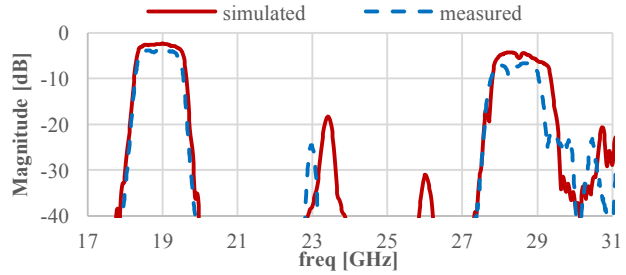

Fig. 9. Simulated and measured transmission parameter ($|s_{21}|$) between ports.

The s_{21} roll-off at the two pass-bands is presented in Fig. 10 using an enhanced logarithmic scale for the abscissa. The logarithm scale takes the frequency band's lower and higher limits as reference. It is seen that the filter has larger than 55 dB/decade roll-off rate at both pass-bands and for both frequency edges, corresponding to more than 10 dB drop per 0.2 GHz.

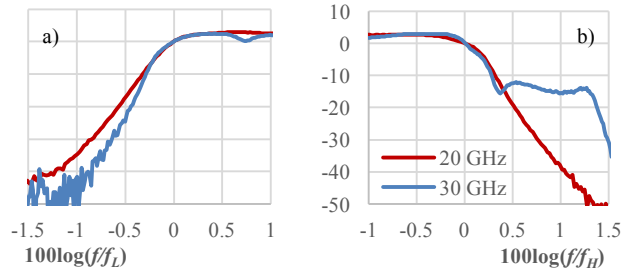

Fig. 10. Magnitude of the measured transmission parameter ($|s_{21}|$) normalized to half power. Abscissae are normalized to both bands' frequency limits: a) lower limits (f_{L20} = 18.4 GHz, f_{L30} = 27.8 GHz); b) higher limits (f_{H20} = 19.5 GHz, f_{H30} = 29 GHz).

IV. Conclusion

A new dual-band filter is proposed for the satellite Ka-band. Simple design guidelines are presented, addressing the bandwidth, pass-band independence between the two sub-waveguides and tuning of both bands.

A prototype was manufactured and characterized experimentally. A 50 dB/decade roll-off was achieved with a 38 × 6.6 × 4.5 mm^3 device. The use of SRRs in a cut-off waveguide configuration proved to be viable for the design of wideband and high selectivity dual-band filters. The second resonant mode of the SRRs embedded in a waveguide demonstrated in [10] proved to be tunable and favorable to high selectivity, controllable bandwidth, and low insertion losses even in a dual-band configuration.

Acknowledgment

The authors acknowledge the collaboration from Carlos Brito and Jorge Farinha for prototype construction and António Almeida for measurements.

References

[1] E. B. Lima, S. A. Matos, J. R. Costa, C. A. Fernandes, and N. J. G. Fonseca, "Circular Polarization Wide-angle Beam Steering at Ka-band by In-plane Translation of a Plate Lens Antenna", *IEEE Trans. Antennas Propag.*, vol. 63, no. 12, pp. 5443-5455, Dec. 2015.

[2] A. Kanso, R. Chantalat, U. Naeem, H. Chreim, M. Thevenot, S. Bila, and T. Monediere; "Multifeed EBG dual-band antenna for spatial mission", *International J. of Antennas and Propag.*, Hindawi Publishing Corporation, Vol. 2011, Article ID 190358, 14 pages, Aug. 2011.

[3] K. Ahn, and I. Yom, "A Ka-band Multilayer LTCC 4-pole Bandpass Filter using Dual-mode Cavity Resonators," Microwave Symposium Digest, 2008 *IEEE MTT-S Intern.*, Atlanta, USA, 2008, pp. 1235-1238.

[4] E. A. Alós, A. U. Zaman, and P.-S. Kildal, "Ka-Band Gap Waveguide Coupled-Resonator Filter for Radio Link Diplexer Application", *IEEE Trans. On Components, Packaging and Manufacturing Technology*, vol. 3, no. 5, May 2013.

[5] Z. Liu, G. Xiao, and L. Zhu, "Triple-Mode Bandpass Filters on CSRR-Loaded Substrate Integrated Waveguide Cavities", *IEEE Trans. on Components, Packaging and Manufacturing Technology*, vol. 6, no. 7, Jul. 2016.

[6] A. K. Horestani, M. Durán-Sindreu, J. Naqui, C. Fumeaux, and F. Martín, "S-Shaped Complementary Split Ring Resonators and Their Application to Compact Differential Bandpass Filters With Common-Mode Suppression", *IEEE Microwave and Wireless Components Letters*, vol. 24, no. 3, Mar. 2014.

[7] B. You, L. Chen, Y. Liang, and X. Wen, "A High-Selectivity Tunable Dual-Band Bandpass Filter Using Stub-Loaded Stepped-Impedance Resonators", *IEEE Microwave and Wireless Components Letters*, vol. 24, no. 11, Nov. 2014.

[8] H. Chu, and J.-X. Chen, "Dual-Band Substrate Integrated Waveguide Bandpass Filter with High Selectivity", *IEEE Microwave and Wireless Components Letters*, vol. 24, no. 6, June 2014.

[9] T. Decoopman, O. Vanbésien, and D. Lippens, "Demonstration of a Backward Wave in a Single Split Ring Resonator and Wire Loaded Finline," *IEEE Microwave Wireless Component Letters*, vol. 14, no. 11, pp. 507 - 509, Nov. 2004.

[10] C. A. Fernandes, R. Marqués, and M. Silveirinha, "Transmission in Rectangular Waveguides Periodically Loaded with SRRs: Simulation and Measurement", *Proceedings of the European Microwave Association*, vol. 2, pp. 66 – 70, March 2006.

[11] R. Marqués, J. Martel, F. Mesa, F. Medina, "A new 2D isotropic Left-handed Metamaterial Design: Theory and Experiment," *Microwave and Opt. Tech. Letters*, vol. 35, no. 5, pp. 406 - 408, 2002.

[12] The Advantage of Nearly Isotropic Dielectric Constant for RT/duroid® 5870-5880 Glass Microfiber-PTFE Composite. Rogers Corporation, U.S.A, 2015. [Online]. Available: https://www.rogerscorp.com/documents/607/acs/The-Advantage-of- Nearly-Isotropic-Dielectric-Constant-of-RT-duroid-5870-5880-Glass-Microfiber-PTFE.pdf.